# Constrained Basis Set Expansions for Target Subspaces in Hyperspectral Detection and Identification

S. Adler-Golden*, J. Gruninger and R. Sundberg
Spectral Sciences, Inc., Burlington MA 01803-3304

## ABSTRACT

Subspace methods for hyperspectral imagery enable detection and identification of targets under unknown environmental conditions (i.e., atmospheric, illumination, surface temperature, etc.) by specifying a subspace of possible target spectral signatures (and, optionally, a background subspace) and identifying closely fitting spectra in the image. The subspaces, defined from a set of exemplar spectra, are compactly expanded in singular value decomposition basis vectors or, less commonly, endmember basis spectra, linear combinations of which are used to fit the image data. In the present study we compared detection performance in the thermal infrared using several different constrained and unconstrained basis set expansions of low-dimensional subspaces, including a method based on the Sequential Maximum Angle Convex Cone (SMACC) endmember algorithm. Constrained expansions were found to provide a modest improvement in algorithm robustness in our test cases.

**Keywords:** hyperspectral, subspace, invariant, detection, infrared

## 1. INTRODUCTION

Hyperspectral imaging (HSI) from airborne or space-based platforms has proven to be a valuable technology for detecting and classifying materials and objects on the Earth's surface based on their spectral signatures. Analysis of these data can be quite challenging, however, as the signatures contain variable atmospheric components and surface spectral properties. In the visible to near-infrared wavelength region there are well-established atmospheric correction or "compensation" methods for converting the HSI data to reflectance spectra, thereby eliminating atmospheric effects.[1-3] In combination with algorithms that account for illumination variation[4] and sub-pixel material mixtures[5], detection, classification and identification can be achieved with the aid of material spectral libraries. For thermal infrared (IR) HSI sensors, analogous methods exist that characterize and remove atmospheric emission and transmittance contributions and retrieve surface emissivity.[6-11] However, these thermal IR algorithms are more complex, less accurate, and often much more computationally intensive due to the need to retrieve additional information on surface and air temperatures.

An alternative analysis approach that may be especially attractive for the thermal IR regime is based on radiance spectrum simulation. Here a comprehensive dataset of potential target spectral signatures, encompassing a sufficiently broad range of atmospheric conditions, surface temperature, etc., is simulated, and the results are compared to the measured pixel spectra. A good match (low residual) strongly suggests that the pixel contains the target in question; a poor match indicates otherwise. The key is to develop a highly efficient matching algorithm, one that does not require numerous case-by-case comparisons.

*sag@spectral.com; phone 1 781 273-4770; fax 1 781 270-1161; spectral.com

In an "invariant" subspace approach described by Healey and Slater[12], the target dataset, which includes all possible sources of variability, is compressed down to a small subspace of orthogonal basis vectors derived from singular value decomposition (SVD). To find a whole-pixel target, the pixel spectra $L$ are fit using this basis set, and an error residual is computed and thresholded. Healey and Slater fit amplitude-normalized pixel spectra and calculate the root-sum-square (RSS) error residual; this is equivalent to normalizing RSS error to the pixel spectrum amplitude, i.e.,

$$\sigma_n = \| L - \sum \alpha_j m_j \| / \|L\| \quad (1a)$$

Here the $m_j$ are the SVD basis vectors, $\alpha_j$ are the coefficients of the fit, and the double bars denote Euclidean norm. The invariant approach was later extended to the detection of subpixel targets by Thai and Healey[13] by modeling the subpixel background as a second subspace, using background SVD basis vectors as additional fitting components. More recent work on subpixel detection has focused on the use of different types of basis sets, including an endmember basis set.[14] It should be noted that one can generate a slightly more efficient subspace basis set by subtracting the mean of the subspace spectra prior to performing the SVD, as is done in a typical principal component analysis. Here the fitting error is not proportional to amplitude, so it is more sensible to use the non-normalized error expression

$$\sigma'_n = \| L' - \sum \alpha'_j m'_j \| \quad (1b)$$

where the $m'_j$ are the SVD basis vectors of the mean-subtracted target subspace, $L'$ is the pixel spectrum after subtraction of the target mean, and the $\alpha'_j$ are the coefficients of the fit to $L'$.

The subspace approach is very flexible, allowing it to be tailored to a variety of remote sensing problems. For example, consider the situation in which atmospheric parameters are known from weather data but range to the target and surface temperature are unknown. Here there are only two dimensions in the target subspace, which can be represented with many fewer SVD basis vectors than the typical ten or so used by Healey *et al.*[12] This reduction in dimensionality may lead to improved detection performance. The subspace approach is also amenable to detecting objects that have intrinsic variability.

One limitation of the above methods is that the size (as distinguished from the dimensionality) of the subspace spanned by the basis vectors is not constrained, since the coefficients $\alpha_j$ (or $\alpha'_j$) are allowed to take on any values. Potentially, non-target spectra might be closely fit with the target basis set using unphysical values of the coefficients, resulting in false detections. In this paper we investigate the use of two different constrained fitting methods that aim to avoid this problem and thereby improve whole-pixel detection performance. In the first method, bounds are placed on the SVD fitting coefficients. That is, the best-fit representation of each pixel is constrained to lie within a hyperrectangle in the SVD coordinate space, whose size and shape are defined by the target dataset. The error of the pixel spectrum fit is then evaluated using the bounded coefficients. We call this method the "constrained SVD method."

In the second method, which we call the "endmember method," non-orthogonal spectral endmembers rather than SVD basis vectors are used to fit the pixel spectra. The endmembers represent extreme points of the target subspace, defining a simplex that closely follows the boundary of the subspace. All targets are represented by positive, sum-to-unity combinations of the endmembers to within a small tolerance. If the fitting of the pixel spectra with the endmembers is performed with both positivity and sum-to-unity constraints, the pixel fits are linear interpolates of the endmembers, and thus lie inside the target simplex. Practical implementation of this method requires an efficient constrained fitting algorithm. We have chosen the sequential projection method used in the SMACC endmember algorithm[15-17], which is faster by an order of magnitude or more than standard constrained least-squares methods. The drawback of this method is that it does not yield a true least-squares solution when the positivity constraint is active. In our initial testing this has posed more of a problem with a high-dimensional target subspace than with a low-dimensional one.

We report here some results from applying both constrained and unconstrained subspace methods to detection of test panels in LWIR imagery taken with the SEBASS hyperspectral sensor.[18] Two different cases are considered: (1) known atmospheric parameters but unknown target range and surface temperature, yielding a two-dimensional target subspace, and (2) three unknown atmospheric parameters and unknown surface temperature, yielding a four-dimensional target subspace.

## 2. METHODOLOGY

### 2.1 Target Subspace Construction

The spectra defining the target subspace are constructed using a standard LWIR/MWIR radiation transport (RT) equation that relates a ground object's surface temperature $T$ and emissivity $e$ to the radiance $L$ measured by a distant sensor:

$$L = e\,t\,B(T) + (1\text{-}e)D(t) + P \qquad (2)$$

All quantities in Eq. (2) are implicitly wavelength-dependent. Here $t$ denotes atmospheric transmittance between the object and the sensor, $B(T)$ is the Planck (blackbody) function of temperature $T$, and $P$ is the path radiance from thermal emission and scattering between the object and the sensor. $D(t)$ represents the downwelling (or environmental) illumination that would be transmitted through the atmosphere and detected at the sensor by an object of unit Lambertian reflectance. These quantities can be calculated from first principles using MODTRAN[19,20] or other RT codes. Although $D(t)$ may contain contributions from ground objects as well as from the sun and sky, the former contribution is very difficult to estimate and is generally neglected, and illumination by a full, clear sky is assumed. Note also that many authors represent $D(t)$ as the product of an incident light flux and the transmittance $t$, but this is not done here, as the product is inexact for non-monochromatic radiation.

A spectrum $L$ synthesized from Eq. (2) is a function of atmospheric conditions, surface temperature $T$, and the emissivity spectrum $e$. At low altitudes of interest, $t$ and $P$ are functions of the column water vapor and lower atmospheric temperature. The variability in these quantities can be modeled reasonably using two dimensions of variation, such as a temperature profile perturbation and a water vapor profile scale factor with respect to a reference atmosphere. The downwelling radiance spectrum $D(t)$ qualitatively resembles $P$ but includes thermal emission from upper atmospheric ozone. While this emission depends on both the ozone concentration and upper atmospheric temperature, it can be modeled simply by scaling the ozone profile. This results in a total of three dimensions of atmospheric variability (temperature, water and ozone) in the spectral radiance $L$.

The final quantities needed to simulate the spectral radiance are the surface temperature $T$ and emissivity $e$. $T$ is presumed to be unknown, adding an additional dimension to the target subspace. Emissivity may be available from a ground truth measurement or retrieved from HSI data using a temperature-emissivity separation (TES) procedure. We use a TES code that is based on the work of Borel.[7,8] This code constructs a three-dimensional look-up table of $t$, $P$ and $D(t)$ covering a wide range of atmospheric conditions, and retrieves emissivity and surface temperature on a pixel-by-pixel basis along with a single set of $t$, $P$ and $D(t)$ spectra appropriate for the scene.

Examples of target subspace spectra are shown in Fig. 1. These spectra, which are for a ~30% reflective (~0.7 emissivity) surface viewed from 1.5 km altitude, correspond to atmospheric conditions defined by our TES code look-up table. With the target subspace thus defined, a small number of basis vectors are found that represent the subspace to within a desired root-mean-square (RMS) accuracy, as described below.

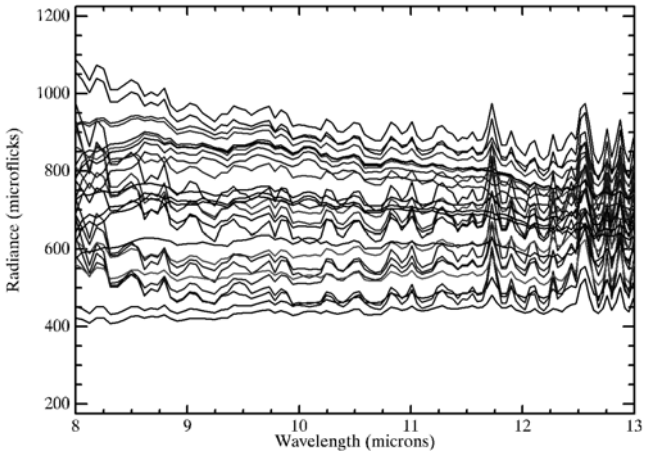


Fig. 1. A sampling of moderate-resolution spectra depicting a ~70% emissive surface over a 40 C temperature range viewed from 1.5 km altitude under a variety of atmospheric conditions.

### 2.2 SVD Basis Set and Fitting Procedure

SVD basis sets for non-mean-subtracted data are obtained as eigenvectors of the target subspace correlation matrix, as in Healey and Slater.[12] Somewhat more efficient basis sets, which represent mean-subtracted target data, may be similarly derived using the target subspace covariance matrix. Since these basis sets are orthonormal, the fitting coefficients in Eqs. (1a) and (1b) are simply the projections of the target spectra onto the basis spectra (from dot products of the data and basis vectors).

In our constrained SVD method, the target subspace spectra are fit with the basis vectors, the extrema of the fitting coefficients for each basis function $j$, denoted $\alpha_{jmin}$ and $\alpha_{jmax}$, are collected, and these values are used to bound the fits of the pixel spectra. That is, pixel spectrum projections less than $\alpha_{jmin}$ or greater than $\alpha_{jmax}$ are reset to $\alpha_{jmin}$ or $\alpha_{jmax}$, respectively, prior to calculation of the error residual. The procedure is the same for both normalized and non-normalized data.

### 2.3 Endmember Basis Set and Fitting Procedure

In the present work, endmember basis sets for the target subspace were derived from the SMACC algorithm.[15-17] This algorithm performs sequential projections to derive both endmembers and their weighting factors (abundances) in the spectral data. The computational steps may be briefly summarized as follows:

1. The largest-amplitude spectrum is selected as the first endmember. When there is no constraint on the weighting factor sum for a given spectrum, provisional weighting factors for this endmember in the data are derived by projection, thereby minimizing the data residual spectra. In the present application, a strict sum-to-unity constraint is desired, so the provisional weighting factors are instead set to 1.
2. The next endmember is selected as the largest-residual spectrum. Provisional weighting factors between 0 and 1 for this endmember in the residual spectra are derived by projection.
3. The data residuals are updated by subtracting from the prior residuals the residual for the new endmember multiplied by the weighting factor for the new endmember in the data. The residual spectrum thus represents the difference between the data spectrum and its representation by a weighted sum of the endmembers determined up to this point.
4. In the updated data spectrum representation, the new endmember replaces a combination of prior endmembers. Therefore, the previously determined weighting factors of the prior endmembers in the data no longer hold and must be updated. In the updating process, the weighting factor is not allowed to become negative. This places an upper limit on the allowable value of the new endmember weighting factor. For spectra that are affected by this limit, the residuals are updated.
5. Steps 2 through 4 are repeated until the residuals are below a threshold or a certain maximum number of endmembers have been selected.

We used a simple variation on this procedure for constrained fitting of the image pixels with the target endmembers, in which the target endmembers are used in steps 1 and 2 instead of newly-selected endmembers. The resulting weighting factors are the fitting coefficients $\alpha'_j$, and the fitting error is calculated from Eq. (1b).

## 3. APPLICATIONS AND RESULTS

We performed our investigation on a hyperspectral image from the airborne SEBASS sensor[18] taken at the Department of Energy's Atmospheric Radiation Monitoring (ARM) site in Lamont, Oklahoma on June, 1997 at 21:21 LT from 1.5 km altitude. The data are described elsewhere.[11] The sensor provides 128 spectral channels from approximately 7.4 to 13.6 μm, of which we typically analyzed those between 8 and 13 μm, where the atmosphere has good transmission. The site, shown in Fig. 2, has various ground covers (grass, water, soil, gravel), buildings, and calibrated emissivity panels. We analyzed two panel targets shown in the image detail, a ~20-30% reflective (70-80% emissive) panel and a near-blackbody panel, the bottom of three similar panels in the rectangle.

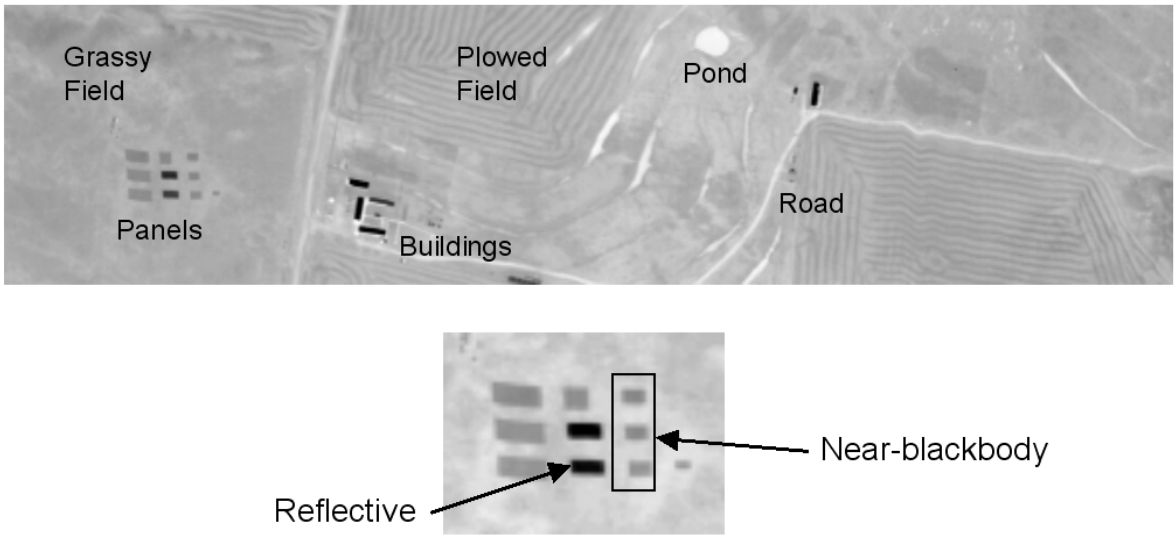


Fig. 2. 11 μm radiance image of the ARM site. Detail shows panels selected as targets.

Our TES code-retrieved emissivity spectra are found to agree quite well with ground truth measurements for various surfaces in the image. For convenience we used retrieved emissivities to define the target subspaces for the detection algorithms.

### 3.1 Case 1: Known Atmospheric Parameters, Unknown Target Range

This test case assumed that the atmospheric profiles, and hence the *t*, *P* and *D(t)* spectra, are reasonably well known, but that the target is at an uncertain distance from the sensor and has an unknown surface temperature. The atmospheric *t*, *P* and *D(t)* spectra were taken from the TES code retrievals. Eq. (2) was then used to construct a target subspace comprised of 30 radiance spectra covering five different surface temperatures (295 to 310 deg K) and six different distances, represented by scaling the *t* and *P* spectra to up to 50% shorter or longer column densities than in the original image. Receiver-operator characteristic (ROC) curves that describe the detection of the panel pixels were constructed by calculating and thresholding the error residual from Eq. (1a) or (1b).

Since our objective is to detect whole-target pixels not only under the particular conditions of the Fig. 2 image, but also under a wide range of conditions, the detection algorithm was run not only on the image but also on the 30-member target subspace, and the total number of correct detections was recorded. Noise added to the image (see below) was included in these subspace spectra. The false positives were taken as the detections in the image outside the target area.

As the reflective panel proved very easy to detect under known atmospheric conditions, and many operational LWIR HSI sensors have poorer signal-to-noise than SEBASS, we generated additional test cases with Gaussian white noise added to the data. The Fig. 3 results, which include 5 μflicks of added noise, show how detection ability varies with the choice and size of the SVD basis set. The curves are labeled with the number of basis vectors included and whether the data are mean-subtracted. The detection metric is the Eq. (1b) error with mean-subtracted data and the Eq. (1a) error with non-mean-subtracted data. However, using the Eq. (1b) error with the latter has little overall effect on the results. Mean subtraction slightly improves the fit to the panel subspace using a given number of basis vectors, so that optimal detection can often be obtained with one less basis vector. However, there is little if any preference for mean subtraction in terms of overall performance. With three basis vectors there is a slight improvement in performance upon constraining the coefficients (compare the solid and dotted lines). With fewer basis vectors the constraint has no effect. The best overall performance is obtained with two basis vectors, which equals the number of subspace dimensions.

Results using endmember basis vectors are shown in Fig. 4 along with some SVD results for comparison. The endmember results are much less sensitive to the number of basis vectors than the SVD results; the four-endmember and seven-endmember ROC curves (solid) overlap over most of their range. In addition, they show comparable performance to the best (two-eigenvector) SVD basis sets. The four-endmember set fits the panel subspace to within 1 μflick, while the seven-endmember set fits to within 0.5 μflick, both values being well below the added noise level.

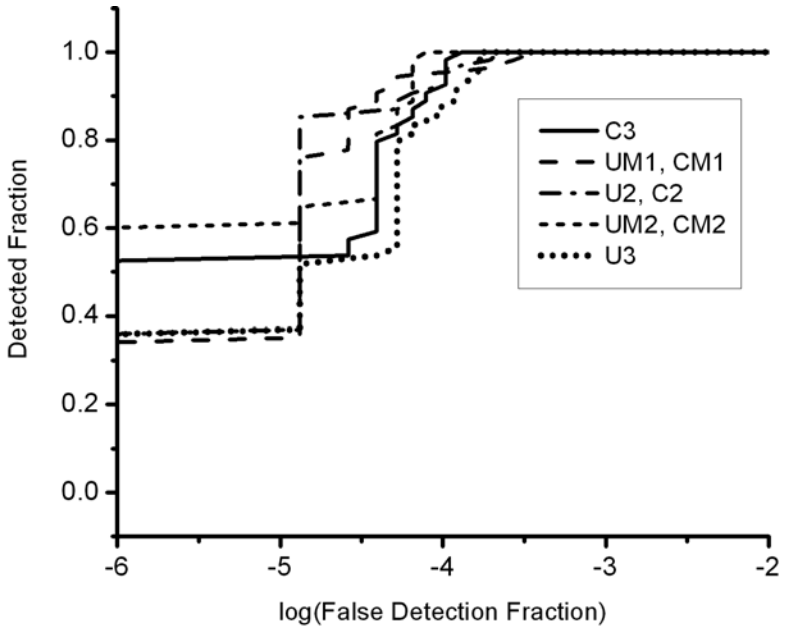


Fig. 3. ROC curves for reflective panel detection at unknown range using various SVD basis sets and numbers of basis vectors. Key: U = unconstrained, C = constrained, M = target mean-subtracted data.

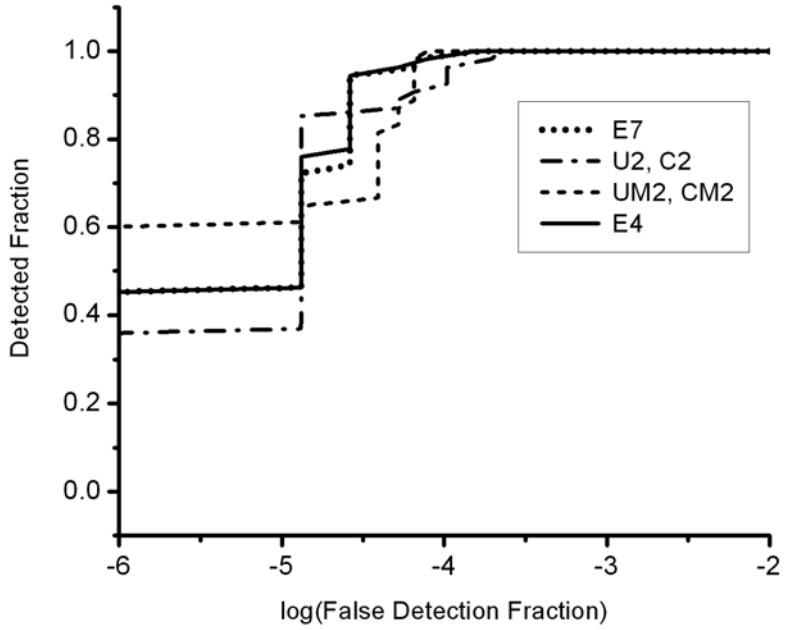


Fig. 4. Comparison of reflective panel ROC curves using endmember (E) basis sets with selected SVD results from Fig. 3.

For the harder-to-detect near-blackbody panel, we added a smaller amount of noise (2 μflicks) to the data. All three panels in the Fig. 2 rectangle are counted as targets. Fig. 5 shows the results with two and three SVD basis vectors. Here, three basis vectors are much better than two, despite the fact that the target subspace is formally two-dimensional. There is no effect from the addition of constraints in this case. The results from six-and eight-endmember basis set, which fits the panel subspace to within respectively 1 and 0.5 μflick, are similar and are as good as the best SVD results.

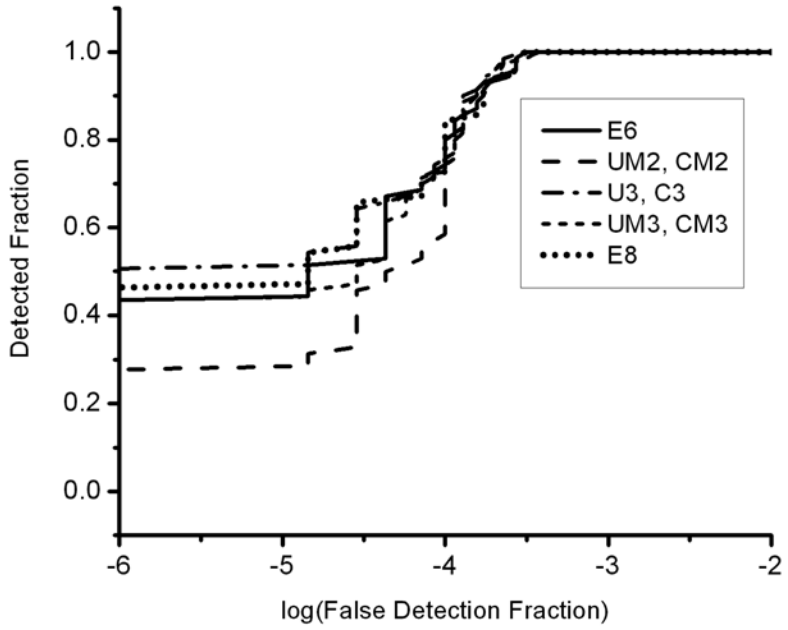


Fig. 5. ROC curves for near-blackbody panel detection at unknown range.

### 3.2 Case 2: Unknown Atmospheric Parameters

For this test case, the target subspace was based on a 60-element, three-dimensional look-up table of atmospheric *t*, *P* and *D(t)* spectra generated by our TES code using MODTRAN. These cover a 40 deg C range in surface air temperature, a factor-of-four range in column water vapor, and factor-of-two range in column ozone. Each *t*, *P*, *D(t)* combination was used in Eq. (2) together with the target emissivity and five surface temperatures, yielding a four-dimensional target subspace containing 300 spectra. Examples of these spectra are in Fig. 1. As in Case 1, 5 μflicks RMS of Gaussian noise has been added to the data.

ROC curve results for detection of the reflective panel are shown in Fig. 6. In contrast to the previous case, here we are searching for only the targets in the image, so the 300 target subspace spectra are not included among those to be detected. The SVD results use mean subtraction and the Eq. (1b) error metric. Very similar results, not shown, were obtained using non-mean-subtracted data with either Eq. (1a) or (1b).

The endmember method ROC curves display little if any variation with the basis set size between 14 and 29 endmembers; only the former is shown (curve with triangles). Their performance is much worse than that of the SVD basis sets (dashed and dotted curves), most likely because the RMS fitting error remains much larger than the noise level. These poor fits may reflect increasing deviation of the SMACC sequential projection scheme from true least-squares results as the number of endmembers increases. Much better fits are however obtained with the near-blackbody target, where our preliminary analysis finds little difference in performance between the endmember and SVD basis sets.

Similar to Case 1, the use of constraints with SVD basis vectors provides little overall difference in performance when the basis set is small. However, the constraints provide a modest improvement with six basis vectors (compare the solid curves U6 and C6) in Fig. 6.

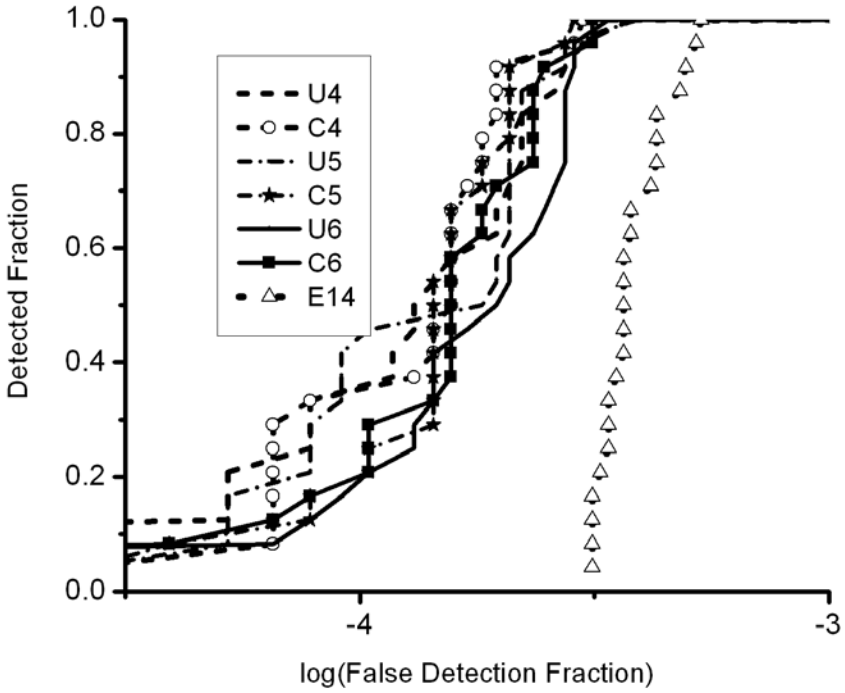


Fig. 6. ROC curves for reflective panel detection under unknown atmospheric conditions.

## 4. SUMMARY AND CONCLUSIONS

This paper describes an application of constrained basis set expansions for target subspaces to whole-pixel detection problems in hyperspectral imagery. Following Healey and Slater[12], the detection metric is taken as a root-sum-square fitting error between the pixel spectrum and its basis set representation. The unconstrained fits use orthogonal basis vectors from an SVD of the target dataset with or without mean subtraction; i.e., the basis vectors are eigenvectors of the correlation or covariance matrix, respectively. One type of constrained fit uses those same basis vectors with the fitting coefficients bounded by those of the target subspace, thereby restricting the fits to the interior of a hyperrectangle in SVD coordinate space. Another type of fit uses endmembers of the target dataset as non-orthogonal basis vectors, and applies sum-to-unity and positivity constraints to constrain the fit to the interior of a simplex. This latter method was implemented using an approximate but fast constrained least-squares procedure.

Two test cases involving thermal IR hyperspectral imagery were considered: (1) known atmospheric parameters but unknown target range and surface temperature, yielding a two-dimensional target subspace, and (2) three unknown atmospheric parameters and unknown surface temperature, yielding a four-dimensional target subspace.

With the two-dimensional subspace, the unconstrained SVD and endmember methods proved comparably effective, but the SVD results were more sensitive to the number of basis vectors. The optimal number of SVD basis vectors corresponds to fitting the target spectra to around the sensor noise level; too many basis vectors result in over-fitting. Similar sensitivity of detection performance to the number of SVD basis vectors in target or background subspaces has been found by other workers.[12-14] Constraining the SVD fit coefficients provided a slight improvement. With the four-dimensional subspace the endmember method gave inconsistent results. Here the constrained SVD method again provided some reduction in basis set sensitivity by improving performance with six basis vectors, although the best performance, obtained with four to five SVD basis vectors, was not improved upon.

Constrained basis set expansions such as those described here may prove to be useful for target detection with other applications or metrics. In particular, they would be applicable to sub-pixel as well as whole-pixel detection when used with background subspace descriptions, which might also be based on constrained expansions.

The present work has not yet addressed the basic question of how subspace and atmospheric correction/TES approaches compare in overall detection performance. This remains a topic for upcoming investigations.

## 5. ACKNOWLEDGEMENTS

The authors are grateful to Dr. J. Romano (US Army ARDEC, Picatinny Arsenal) for program guidance and Drs. Marsha Fox and Lawrence Bernstein (Spectral Sciences, Inc.) and Alan Stocker (Space Computer Corp.) for helpful technical discussions. This work was funded by the US Army under Contract No. W15QKN-07-C-0008.

## 6. REFERENCES

1. M.W. Matthew , S.M. Adler-Golden, A. Berk, G. Felde, G.P. Anderson, D. Gorodetzky, S. Paswaters and M. Shippert, "Atmospheric Correction of Spectral Imagery: Evaluation of the FLAASH Algorithm with AVIRIS Data," *SPIE Proc, Algorithms and Technologies for Multispectral, Hyperspectral, and Ultraspectral Imagery IX* (2003).
2. R. Richter, "Atmospheric/Topographic Correction for Airborne Imagery," ATCOR-4 Users Guide, Version 4.0 (January 2005).
3. A. Qu, B. C. Kindel, and A. F. H. Goetz, "The High Accuracy Atmospheric Correction for Hyperspectral Data (HATCH) Model," *IEEE Trans. Geoscience Remote Sensing*, **41**, 1223-1231 (2003).
4. S.M. Adler-Golden, R.Y. Levine, M.W. Matthew, S.C. Richtsmeier, L.S. Bernstein, J.H. Gruninger, G. Felde, M. Hoke, G.P. Anderson, and A. Ratkowski, "Shadow-Insensitive Material Detection/Classification with Atmospherically Corrected Hyperspectral Imagery," *Proc. of SPIE*, Orlando, FL, Vol. 4381-51 (April 2001).
5. D. Manolakis and G. Shaw, "Detection Algorithms for Hyperspectral Imaging Applications," IEEE Signal Processing Magazine, **19**, Issue 1, pp. 29-43 (2002).
6. M. Boonmee, J.R. Schott and D.W. Messinger, "Land surface temperature and emissivity retrieval from thermal infrared hyperspectral imagery," *Algorithms and Technologies for Multispectral, Hyperspectral, and Ultraspectral Imagery XII*, Sylvia Shen and Paul Lewis, eds., *Proc. SPIE* **6233**, 62331V (2006).
7. C.C. Borel, "ARTEMISS – an Algorithm to Retrieve Temperature and Emissivity from Hyper-Spectral Thermal Image Data," *28th Annual GOMACTech Conference, Hyperspectral Imaging Session*, Tampa, FL, Los Alamos National Lab. Rpt. No. LA-UR-027907 (2003).
8. C.C. Borel, "Surface emissivity and temperature retrieval for a hyperspectral sensor," in *IGARSS 1998*, IEEE International Geoscience and Remote Sensing Symposium, **1**, pp. 546-549 (1998).
9. D. Gu, A.R. Gillespie, A.B. Kahle and F.D. Palluconi, "Autonomous atmospheric compensation (AAC) of high resolution hyperspectral thermal infrared remote-sensing imagery," *IEEE Trans. Geosci. Remote Sens.*, **38**, 2557-2570 (2000).
10. E.D. Hernandez-Baquero and J. R. Schott, "Atmospheric compensation for surface temperature and emissivity separation," *SPIE Proceedings, Algorithms for Multispectral, Hyperspectral, and Ultraspectral Imagery VI*, Vol. 4049, pp. 400-410 (2000).
11. S.J. Young, B.R. Johnson and J.A. Hackwell, "An In-scene Method for Atmospheric Compensation of Thermal Hyperspectral Data," *J. Geophys. Res. Atmospheres*, Vol. 204, pp. ACH 14-1 – ACH 14-20 (2002).
12. G. Healey and D. Slater, "Models and Methods for Automated Material Identification in Hyperspectral Imagery Acquired Under Unknown Illumination and Atmospheric Conditions," IEEE Trans. Geosci. Remote Sensing, 37, 2706-2717 (1999).
13. B. Thai and G. Healey, "Invariant Subpixel Material Detection in Hyperspectral Imagery," IEEE Trans. Geosci. Remote Sensing, **40**, 599-608 (2002).
14. P. Bajorski, E.J. Ientilucci and J.R. Schott, "Comparison of Basis-Vector Selection Methods for Target and Background Subspaces as Applied to Subpixel Target Detection," *Algorithms and Technologies for Multispectral, Hyperspectral, and Ultraspectral Imagery X*, Sylvia Shen and Paul Lewis, eds., *Proc. SPIE* **5425**, 97-108 (2004).
15. J. Gruninger and S. Adler-Golden, "Process for Finding Endmembers in an Image," U.S. Patent Pending (2006).
16. J.H. Gruninger, J. Lee and R.L. Sundberg, "The Application of Convex Cone Analysis to Hyper-spectral and Multi-spectral Scenes," *SPIE 9th International Symposium on Remote Sensing* Crete, Greece, Vol. 4885-25, 23-27 September (2002)
17. J.H. Gruninger , A.J. Ratkowski, and M.L. Hoke, "The Sequential Maximum Angle Convex Code (SMACC) Endmember Model," *Algorithms and Technologies for Multispectral, Hyperspectral, and Ultraspectral Imagery X*, Sylvia Shen and Paul Lewis, eds., *Proc. SPIE* **5425**, 1-14 (2004).
18. J.A. Hackwell, D.W. Warren, R.P. Bongiovi, S.J. Hansel, T.L. Hayhurst, M.G. Sivjee, and J.W. Skinner, "LWIR/MWIR imaging hyperspectral sensor for airborne and ground-based remote sensing," *SPIE Proceedings, Imaging Spectrometry*, Vol. 2819, pp. 102-107 (1996).

19. A. Berk, L.S. Bernstein, G.P. Anderson, P.K. Acharya, D.C. Robertson, J.H. Chetwynd and S.M. Adler-Golden, “MODTRAN Cloud and Multiple Scattering Upgrades with Application to AVIRIS,” *Remote Sens. Environ.* 65:367-375 (1998).
20. A. Berk, P.K. Acharya, L.S. Bernstein, G.P. Anderson, J.H. Chetwynd, and M.L. Hoke, “Reformulation of the MODTRAN band model for higher spectral resolution,” *SPIE Proceeding,* A*lgorithms for Multispectral, Hyperspectral, and Ultraspectral Imagery VI*, Vol. 4049 (2000).